

Powder Bed Fusion of Nontoxic Copper(I) Sulfide Thermoelectric Materials for Energy Harvesting

Raden Gustinvil¹, Giuseppe L. Di Benedetto², Donald Skelton², Samuel Stuart³, and Emrah Celik¹

¹Mechanical and Aerospace Engineering Department
University of Miami
Coral Gables, FL, USA, 33146

²U.S. Army Combat Capabilities Development Command
Armaments Center, Picatinny Arsenal, NJ 07806, USA

³U.S. Navy Naval Surface Warfare Center, Crane Division, IN 47522, USA

Contact Author Email: e.celik.miami.edu

Abstract

Copper(I) sulfide (Cu₂S) has gained significant appeal as a thermoelectric material recently, since it is an earth-abundant, nontoxic material with high conversion efficiency in the middle-high temperature range (>650 K). Melting-based manufacturing of copper(I) sulfide, however, leads to the sulfur deficiency and dramatic reduction of its thermoelectric performance. In this study, we present the use of powder bed fusion (PBF) additive manufacturing technology to fabricate Cu_{2-x}S samples with high thermoelectric performance for the first time. PBF allows enhanced designed freedom and the following sulfur infusion postprocessing reverts the impaired thermoelectric properties back to its original state. Thermoelectric characterization of the fabricated specimens indicated a p-type material with peak electrical conductivity of 115 Scm⁻¹ at 650 K, Seebeck coefficient of 182 μVK⁻¹ at 775 K, and a power factor of 0.34 mWm⁻¹K⁻² at 775 K. This is the first report of Cu_{2-x}S fabricated using this additive manufacturing methodology and with high thermoelectric performance. This work demonstrates the importance of the sulfur infusion postprocessing to revert the lost sulfur thus enhancing the energy conversion efficiency. Fabrication of environmentally friendly thermoelectric materials with extended design freedom and at high conversion efficiency has the potential to greatly impact the thermoelectric industry with novel energy harvesting applications and lowered manufacturing costs.

Keywords

Powder bed fusion; Copper(I) sulfide; 3D printing; Thermoelectrics; Sulfur infusion

Introduction

The direct and thermodynamically reversible conversion of heat energy into electrical energy and vice versa is commonly referred to as thermoelectricity [1]. Thermoelectric (TE) materials use this phenomenon in thermoelectric generators (TEG) to improve energy efficiency in a variety of systems by recapturing surplus heat that would otherwise be wasted to the environment. To measure the performance of various thermoelectric materials, the dimensionless figure of merit, ZT , is used:

$$ZT = \frac{\sigma S^2}{\kappa} T$$

where σ is the electrical conductivity, S is the Seebeck coefficient, κ is the thermal conductivity and T is the absolute temperature in Kelvin.

The thermoelectric phenomenon has garnered significant scientific interest since the 1950s [2]. The most common and widely known materials for commercial thermoelectric applications being from the chalcogen family specifically: bismuth telluride (Bi₂Te₃) [3, 4] and lead telluride (PbTe) [5, 6] as they have been reported to have a ZT value around one in low to medium range temperature settings. Although these are currently the most used TE materials for commercial applications, these materials are highly toxic and expensive. Copper-based chalcogenides, specifically copper sulfides, address these issues. Copper sulfides are an earth abundant, non-toxic, and compositionally versatile class of materials with a high ZT level [7].

Copper(I) sulfide (Cu₂S), often known as chalcocite, has three different crystal phases. Monoclinic $P21/c$ crystal structure of γ -Cu₂S below 370 K, hexagonal β -Cu₂S between 370 and 700 K, and cubic α -Cu₂S phase above 700 K (. With reported values of a maximum ZT of 1.7 at 1000 K for bulk solids [8], copper(I) sulfide has previously been shown to be an effective substitute as a thermoelectric material. However, it has one of the more complicated phase diagrams of any metal sulfide, making it challenging to synthesis with stoichiometric precision [9] throughout the full composition range. The stoichiometry and thermoelectric characteristics of Cu₂S are strongly connected. Under the correct circumstances, the mobility of copper ions can increase copper surface migration above the superionic phase transition temperature (~350 K), which influences the conversion efficiency. This can be reduced by either reducing the operating current or adding a grain-boundary designed microstructure. Consequently, permitting the transport of electrons and holes while obstructing the transit of ions [10].

Traditional TE leg fabrication involves powder synthesis, sintering or ingot pressing, leg dicing, metallization, and interconnect fabrication [11]. There are fundamental limitations, however, to thermoelectric systems preventing

their integration into modern society including low conversion efficiency and this complex multistep fabrication process. The procedure is time consuming, costly, and limited to simple planar geometric structures. Three-dimensional (3D) printing technologies offer a transformative potential for manufacturing the next generation of TE systems by overcoming these challenges. Various additive manufacturing (AM) technologies have been previously implemented for the fabrication of TE materials including fused filament fabrication [12], stereolithography [13], and powder bed fusion [14]. Powder bed fusion (PBF), also known as selective laser sintering/melting, is an additive manufacturing process that allows for the generation of complex parts by selectively solidifying layers of powder material on top of each other by means of a high-power laser. In the build chamber, a thin layer of powder typically 40-60 microns [15] is spread across the print bed and the laser is directed onto specific regions to fuse the powder together. Afterwards, the platform is moved down a predetermined distance where the entire process is repeated until the final part is complete. Polymers [16], metals [17], and ceramics [18] have been fabricated using this technology. The only report work of additively manufactured Cu_{2-x}S was accomplished using a pseudo 3D printing paste extrusion technique with a maximum ZT of 0.63 at 966 K [19]. In this work we present the first successfully demonstrated use of a commercial PBF printer (EOS M100) with a modified recoater blade capable of processing irregularly shaped Cu_2S powder feedstock.

Methodology

Sample Fabrication: Commercial copper(I) sulfide (Cu_2S) powder (American Elements, 99.995%) was sieved using a vibratory sieve shaker (Gilson, Lewis Center, OH) to a particle size distribution of $\sim 20 - 45 \mu\text{m}$. The PBF process was conducted using an EOS M100 (EOS, Krailling, Munich) with a customized vibratory recoater blade as shown in Figure 1. The machine is equipped with a 200 W Yb fiber laser with a focus spot size of $40 \mu\text{m}$. Samples were printed in various geometries with a layer height of 20 microns on a stainless-steel $\varnothing 100 \text{ mm}$ substrate.

Sulfur Infusion Postprocessing: Due to the high energy input from the laser, sulfur in the alloy volatilizes, causing the sample to become sulfur deficient. After the sintering process, copper precipitates can be observed within the cross section of the sample. This decreases the sample's thermoelectric performance. Postprocessing was applied to infuse sulfur back into the specimens and enhance thermoelectric properties. The sintered specimens were heated at 1073 K, well below the sintering temperature of copper(I) sulfide, for 2 hours with sulfur powder (99.5%, Alfa Aesar) in the vacuum sealed furnace and purged with argon gas to diffuse the lost sulfur back into the system. For post-processing, five percent of the total mass of the sample in sulfur was utilized.

Compositional Characterization: Scanning electron microscopy (SEM) was conducted on as-is and post-processed samples with images taken on the Zeiss Gemini Field Emission SEM (Germany). Sputter coating was not required due to the conductive nature of the samples.

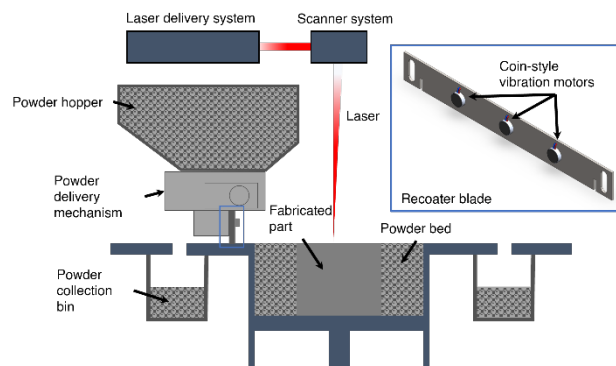


Figure 1: Schematic overview of PBF process

Thermoelectric Characterization: Electrical conductivity and Seebeck coefficient were measured using the Linseis LSR-3 system (Linseis, Germany). Electrical conductivity was calculated using the measured resistivity of the sample via the four-point probe method with a current of 10 mA being applied through the upper and lower electrodes at the time of measurement. The voltage was recorded in the middle of the sample by two (2) affixed thermocouples. Seebeck coefficient measurements were conducted using an upper and lower heater maintaining a constant thermal gradient of 30 K. The voltage and temperature differential were recorded using the same platinum-coated thermocouples spaced approximately three (3) mm apart. All measurements were performed from room temperature to 774 K in 25 K intervals with a heating rate of 10 Kmin^{-1} . Properties were probed three (3) times at each temperature point with a dwell time of one (1) minute in-between each consecutive measurement. Density (ρ) of the 3D-printed samples were measured using a density determination kit (Ohaus, Parsippany, NJ) based on the Archimedes' principle. For the thermoelectric characterization, sample dimensions were required to have a minimum thickness of two (2) mm, a height of seven (7) mm and a width of four (4) mm.

Parameter Optimization: Prior to fabricating thermoelectric specimens, optimal printing parameters must be obtained for the Cu_2S powder in the EOS M100 machine. The energy density given by the equation:

$$E = \frac{P}{vht}$$

where P is the laser power (W), v is the scan speed (mm s^{-1}), t is the layer height (mm), and h is the hatch distance (mm) needed to be identified. These parameters can be optimized by conducting a single line test varying the laser power and scan speed while visually identifying the appropriate melt pool width. Laser speed was assessed

from 25 – 175 W in 25 W increments while scan speed was tested from 200 – 1600 mm s^{-1} in 200 mm s^{-1} increments as shown in Figure 2. The laser parameters chosen were 30W, 400 mm s^{-1} , and a hatch distance of 0.07 mm and layer thickness of 0.02 mm giving a volumetric energy density of 53.57 Jmm^{-3} .

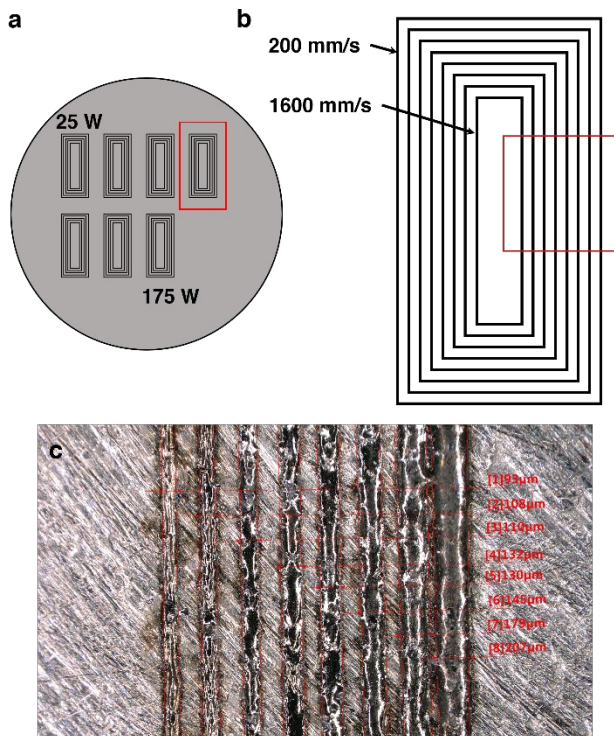


Figure 2: Single line test conducted with a single layer of Cu_2S powder. a) Arrangement of test on print substrate. b) Layout of scan lines. c) Melt pool width analysis conducted using FIJI

Results

Morphological Analysis: Using the obtained parameters, samples were fabricated in various complex geometries with a total of 100 layers yielding an approximate height of two (2) mm. As shown in Figure 3, these features would otherwise be difficult to fabricate using traditional manufacturing methodologies. Samples were found to be highly dense with a density of $5.422 \pm 0.291 \text{ gcm}^{-3}$ after post processing. No separation of the subsequent layers was present in the cross section of the sample indicating full melting of each layer was achieved. The internal defects in Figure 3d can be attributed to gas entrapment [ref] due to the rapid solidification during the PBF process.

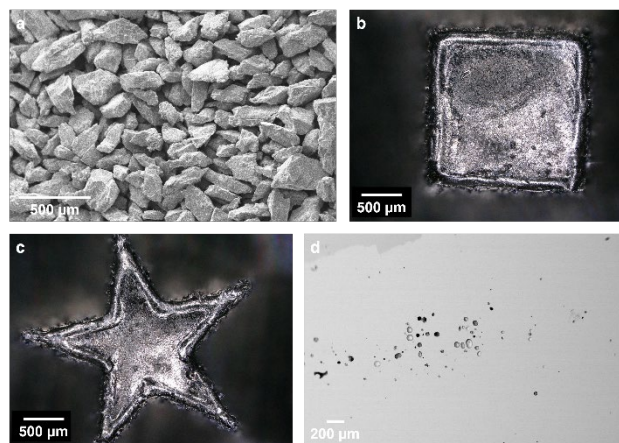
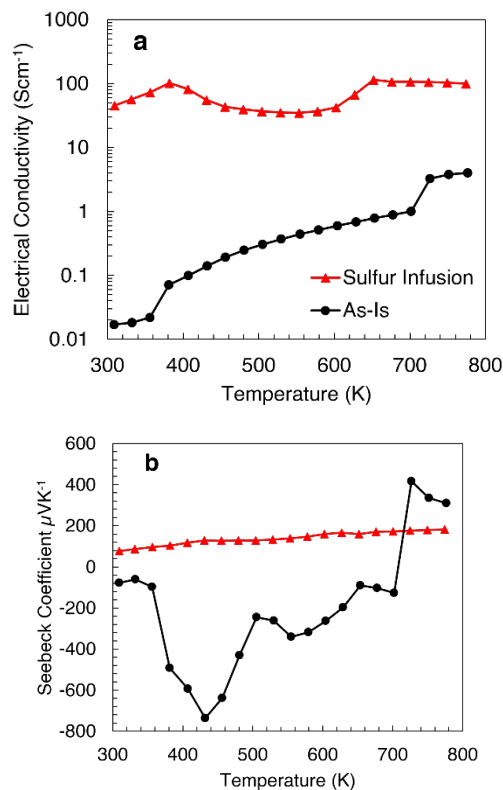


Figure 3: a) Cu_2S feedstock powder. b-c) Samples fabricated in the EOS M100 in various geometries. d) SEM of a polished cross section of the post processed sample.

Thermoelectric Characterization: Figure 4 displays the electrical conductivity, Seebeck coefficient and power factor of the as-is and sulfur infused samples. Electrical conductivity (displayed in log scale) ranged from 35 to 115 Scm^{-1} for post processed samples and from 0.02 to 4 Scm^{-1} for as printed samples. Seebeck coefficient varied from 76 to $X 182 \mu\text{VK}^{-1}$ for post process samples and -736 to $416 \mu\text{VK}^{-1}$ for as printed samples. Between 370 – 700 K the cause for printed samples acting as a n-type could be due the increased mobility of copper ions and the excess electrons associated with it.



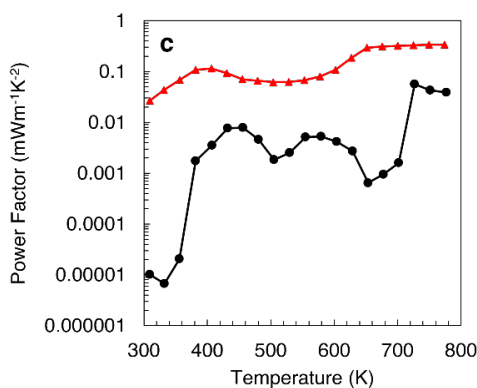


Figure 4: Thermoelectric properties of PBF fabricated Cu_{2-x}S samples: a) electrical conductivity, b) Seebeck coefficient, and c) power factor.

The effect of transitioning from copper-rich to sulfur-rich material can be so dramatic that the power factor increases two orders of magnitude as reported here.

Conclusion

The work presented here exhibits the first successful use of a commercial PBF system to produce Cu_{2-x}S samples using irregularly shaped powder. Using a sulfur infusion post processing method, samples' stoichiometry transition from copper rich to sulfur rich marked by a significant increase in thermoelectric properties. Post processed samples demonstrated a peak electrical conductivity of 115 Scm^{-1} at 650 K, Seebeck coefficient of $182 \mu\text{VK}^{-1}$ at 775 K. Leading to a power factor of $0.34 \text{ mWm}^{-1}\text{K}^{-2}$ at 775 K, the highest reported for Cu_{2-x}S bulk samples made using this AM methodology.

Acknowledgements

This work is supported by the U.S. Army Combat Capabilities Development Command Armaments Center under the Project Number DOTC-19-01-INIT0903.

References

1. Twaha, S., et al., *A comprehensive review of thermoelectric technology: Materials, applications, modelling and performance improvement*. Renewable and Sustainable Energy Reviews, 2016. **65**: p. 698-726.
2. Beretta, D., et al., *Thermoelectrics: From history, a window to the future*. Materials Science and Engineering: R: Reports, 2019. **138**.
3. Goldsmid, H.J., *Bismuth Telluride and Its Alloys as Materials for Thermoelectric Generation*. Materials, 2014. **7**(4): p. 2577-2592.
4. Poudel, B., et al., *High-thermoelectric performance of nanostructured bismuth antimony telluride bulk alloys*. Science, 2008. **320**(5876): p. 634-638.
5. Dughaish, Z.H., *Lead telluride as a thermoelectric material for thermoelectric power generation*. Physica B-Condensed Matter, 2002. **322**(1-2): p. 205-223.
6. LaLonde, A.D., et al., *Lead telluride alloy thermoelectrics*. Materials Today, 2011. **14**(11): p. 526-532.
7. Liu, W.D., et al., *Promising and Eco-Friendly Cu_2X -Based Thermoelectric Materials: Progress and Applications*. Adv Mater, 2020. **32**(8): p. e1905703.
8. He, Y., et al., *High thermoelectric performance in non-toxic earth-abundant copper sulfide*. Adv Mater, 2014. **26**(23): p. 3974-8.
9. Dennler, G., et al., *Are Binary Copper Sulfides/Selenides Really New and Promising Thermoelectric Materials?* Advanced Energy Materials, 2014. **4**(9).
10. Qiu, P., et al., *Suppression of atom motion and metal deposition in mixed ionic electronic conductors*. Nat Commun, 2018. **9**(1): p. 2910.
11. Zhang, H., et al., *Laser additive manufacturing of powdered bismuth telluride*. Journal of Materials Research, 2018. **33**(23): p. 4031-4039.
12. Oztan, C., et al., *Additive manufacturing of thermoelectric materials via fused filament fabrication*. Applied Materials Today, 2019. **15**: p. 77-82.
13. Orrill, M. and S. LeBlanc, *Printed thermoelectric materials and devices: Fabrication techniques, advantages, and challenges*. Journal of Applied Polymer Science, 2017. **134**(3).
14. Thimont, Y., et al., *Thermoelectric Higher Manganese Silicide: Synthesized, sintered and shaped simultaneously by selective laser sintering/Melting additive manufacturing technique*. Materials Letters, 2018. **214**: p. 236-239.
15. Vock, S., et al., *Powders for powder bed fusion: a review*. Progress in Additive Manufacturing, 2019. **4**(4): p. 383-397.
16. Chatham, C.A., T.E. Long, and C.B. Williams, *A review of the process physics and material screening methods for polymer powder bed fusion additive manufacturing*. Progress in Polymer Science, 2019. **93**: p. 68-95.
17. Oliveira, J.P., A.D. LaLonde, and J. Ma, *Processing parameters in laser powder bed fusion metal additive manufacturing*. Materials & Design, 2020. **193**.
18. Florio, K., et al., *Process characterization and analysis of ceramic powder bed fusion*. International Journal of Advanced Manufacturing Technology, 2021. **117**(7-8): p. 2105-2116.
19. Burton, M.R., et al., *Earth abundant, non-toxic, 3D printed Cu_{2-x}S with high thermoelectric figure of merit*. Journal of Materials Chemistry A, 2019. **7**(44): p. 25586-25592.